

Article

Aerosol Particle Transport and Deposition in Upper and Lower Airways of Infant, Child and Adult Human Lungs

Md. M. Rahman ^{1,2,*} , Ming Zhao ^{1,*} , Mohammad S. Islam ³ , Kejun Dong ⁴  and Suvash C. Saha ³

¹ School of Engineering, Design and Built Environment, Western Sydney University, Penrith, NSW 2751, Australia

² Department of Mathematics, Faculty of Science, Islamic University, Kushtia 7003, Bangladesh

³ School of Mechanical and Mechatronic Engineering, University of Technology Sydney, Ultimo, NSW 2007, Australia; mohammadsaidul.islam@uts.edu.au (M.S.I.); Suvash.Saha@uts.edu.au (S.C.S.)

⁴ Center for Infrastructure Engineering, Western Sydney University, Penrith, NSW 2751, Australia; Kejun.Dong@westernsydney.edu.au

* Correspondence: 19615253@student.westernsydney.edu.au (M.M.R.); M.Zhao@westernsydney.edu.au (M.Z.)

Abstract: Understanding transportation and deposition (TD) of aerosol particles in the human respiratory system can help clinical treatment of lung diseases using medicines. The lung airway diameters and the breathing capacity of human lungs normally increase with age until the age of 30. Many studies have analyzed the particle TD in the human lung airways. However, the knowledge of the nanoparticle TD in airways of infants and children with varying inhalation flow rates is still limited in the literature. This study investigates nanoparticle ($5 \text{ nm} \leq d_p \leq 500 \text{ nm}$) TD in the lungs of infants, children, and adults. The inhalation air flow rates corresponding to three ages are considered as $Q_{in} = 3.22 \text{ L/min}$ (infant), 8.09 L/min (Child), and $Q_{in} = 14 \text{ L/min}$ (adult). It is found that less particles are deposited in upper lung airways (G0–G3) than in lower airways (G12–G15) in the lungs of all the three age groups. The results suggest that the particle deposition efficiency in lung airways increases with the decrease of particle size due to the Brownian diffusion mechanism. About 3% of 500 nm particles are deposited in airways G12–G15 for the three age groups. As the particle size is decreased to 5 nm, the deposition rate in G12–G15 is increased to over 95%. The present findings can help medical therapy by individually simulating the distribution of drug-aerosol for the patient-specific lung.

Keywords: particle transport and deposition (TD); airway reduction; drug-aerosol delivery; aging effect; lung generations; diffusion mechanism



Citation: Rahman, M.M.; Zhao, M.; Islam, M.S.; Dong, K.; Saha, S.C. Aerosol Particle Transport and Deposition in Upper and Lower Airways of Infant, Child and Adult Human Lungs. *Atmosphere* **2021**, *12*, 1402. <https://doi.org/10.3390/atmos12111402>

Academic Editor: Deborah Traversi

Received: 28 September 2021

Accepted: 22 October 2021

Published: 26 October 2021

Publisher's Note: MDPI stays neutral with regard to jurisdictional claims in published maps and institutional affiliations.



Copyright: © 2021 by the authors. Licensee MDPI, Basel, Switzerland. This article is an open access article distributed under the terms and conditions of the Creative Commons Attribution (CC BY) license (<https://creativecommons.org/licenses/by/4.0/>).

1. Introduction

Inhalation of aerosol particles is employed directly as a drug delivery method for the treatment of lung diseases [1,2]. However, the effectiveness of particle deposition as a drug delivery depends on particle size, shape, and breathing capacity [3]. Therefore, a detailed understanding of particle deposition in the human lung airways is important for human health to measure both the efficiency of inhaled drug therapy and the health implications of air pollution.

Many researchers have studied nanoparticles deposition in human lung models to investigate the diffusion mechanism [4–8]. The results revealed that the percentage of nanoparticles deposited in the deep airways was greater than microparticles. Cheng, et al. [9] found significant amount of particles are deposited in bifurcation areas by conducting experiments of nanoparticle deposition in the nasal and oral airways. Balásházy and Hofmann [10] studied numerically the deposition of 10-nm diameter particles in the third and fourth generation of human lungs based on the Weibel model [11]. They found significant effects of flow rate and particles size on the deposition efficiency. The whole human respiratory system is made up of 23 generations (the number of divisions of

bronchioles is called generation) of airway branches (G0–G23). Moskal and Gradoń [12] conducted numerical simulations of the TD of 10 nm and 100 nm particles in the first two bifurcations of a symmetric lung model. The study explained the flow pattern and particle deposition through flow visualizations. The numerical study of the particle TD in the third and fourth generation conducted by Hofmann, et al. [13] demonstrated that in the range of $1 \text{ nm} \leq d_p \leq 500 \text{ nm}$, more small size nanoparticles is deposited in the lung airways than large size nanoparticles. CFD simulations of a realistic lung model from generations G0 to G6 were performed by Pourmehran, et al. [14]. Using Large Eddy Simulations (LES), Islam, et al. [15] simulated nanoparticle transport in lung models of up to 17 generations and discussed the total deposition efficiency of particles across the 17 generations. Asgari, et al. [16] investigated aerosol microparticle deposition in a realistic lung model of generations mouth to sixth generations (G6). The results showed that aerosol deposition happens mainly in the upper lung airway.

The lung airways get larger as people grow to adult, and the shape of alveoli changes [17]. During postnatal growth, tidal and residual volumes, respiration rate, and respiratory compliance rise, but respiratory resistance decreases [18]. This is due to the fact that infants and children have immature and growing lung systems, higher physical activity levels, and lower body weight than adults [19,20]. The airway structure and breathing habits of children are different from adults [21]. When it comes to aerosol inhalation treatment, infants and children constitute a distinct demographic of patients [22]. Xu and Yu [23] established a theoretical model for predicting inhaled aerosol TD in the respiratory tracts of children to adults and found that children had a higher deposition efficiency in the upper airway region than adults.

Most medications were developed and approved based on adult trials. There is relatively little information on the acceptability of different dose forms based on a children. As a result, it is important to understand and improve particle TD in infants' and children's lungs.

Lung airway branching pattern is different irrespective of age and sex. The lack of high-resolution CT images also makes the geometry generation process complicated. As a result, it is nearly impossible to generate an age-specific realistic lung model with consistent similar branching patterns. Therefore, the age-specific micro-particles deposition into the idealized lung airways model has been studied through CFD simulation [24,25].

The nanoscale aerosol particle TD as a drug delivery method into deep lung airways is significant for treating lung diseases. Therefore, this study analyses the age-specific different nanoparticles TD in an upper and lower (pulmonary) airway to ensure particles go through the deep lung airways. In addition, it aims to understand the airflow characteristics, wall shear effect, pressure drop, and particle deposition rate for infant, child, and adult people through CFD simulations. The outcome of this investigation will provide quantitative insight into how particle TD is affected by particle size and age.

2. Lung Model

2.1. Lung Geometry

According to the age categories used by the World Health Organization [26,27], we consider 9-month, 6-year, and 30-year-old people as infants, children, and adults, respectively. Weibel, et al. [11] developed planar and symmetric lung models of adult people. However, the lung airway branching patterns for different ages of people are different. Therefore, Xu and Yu [23] developed mathematical description of symmetric lung airways structure for different ages people. We have calculated the details of the lung airways diameter and length for infants, children, and adults (in Table 1) based on the mathematical description [23]. The right-hand side of Figure 1 shows three-dimensional (3D) lung models for upper (G0–G3) and lower generation (G12–G15) that are constructed using SolidWorks software. The detailed geometric parameters of infant, child, and adult lung airways are listed in Table 1.

Table 1. The parameters of symmetric lung airways [23].

Generation (G)	Diameter (cm)	Length (cm)	Diameter (cm)	Length (cm)	Diameter (cm)	Length (cm)
Upper airways (G0–G3)	9 month old infant		6 year old child		30 year old adult	
0	0.615	4.630	0.985	7.934	1.665	12.286
1	0.491	1.712	0.842	2.822	1.219	4.284
2	0.333	0.761	0.572	1.307	0.829	1.896
3	0.227	0.307	0.387	0.525	0.559	0.759
Lower airways (G12–G15)						
12	0.041	0.143	0.067	0.233	0.095	0.330
13	0.036	0.121	0.058	0.193	0.082	0.271
14	0.031	0.097	0.052	0.161	0.074	0.231
15	0.028	0.087	0.046	0.142	0.066	0.201

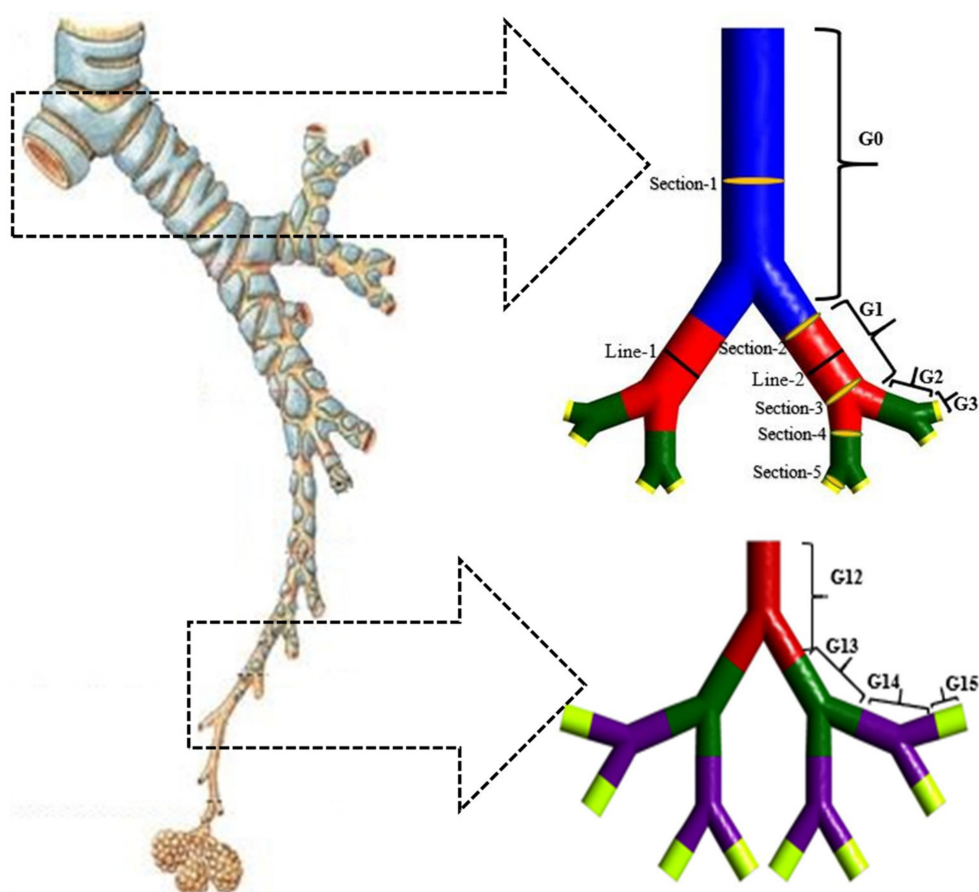


Figure 1. Symmetric models [11] (right) were used in this study to represent the human respiratory system provided by Zhang, et al. [28] (Permission has been taken to use the left figure). The details of the geometric parameters of the lung airways are presented in Table 1.

2.2. Mesh Generation

High resolution mesh in the lung airways has been developed and shown in Figure 2a. In addition, Ten-layer smooth inflation is implemented near the wall to accurately predict the wall boundary flow inside the lung airway, as illustrated in Figure 2b.

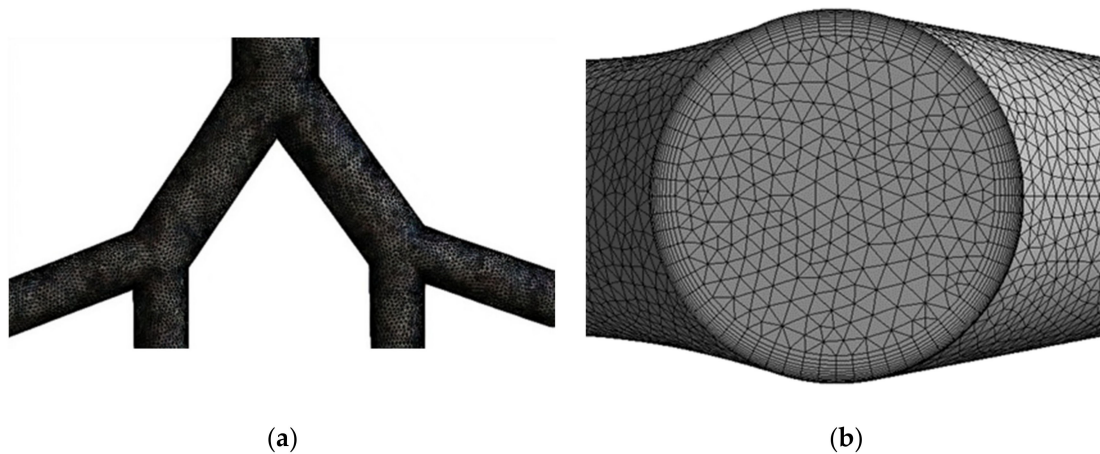


Figure 2. An overview mesh generation for symmetric lung model. (a) The mesh resolution of lung airway and (b) the refined inflation mesh near the airway wall.

3. Numerical Method

3.1. Airflow Model

The airflow in airways is solved using the software ANSYS FLUENT. The maximum Reynolds numbers based on the airway diameter at G0 are 800, 1253, and 1281 for 9-month, 6-year, and 30-year ages, respectively. The flow for such small Reynolds numbers was assumed steady and laminar. The governing equations for solving the flow is the 3D Navier-Stokes equations:

$$\frac{\partial}{\partial x_i} (\rho u_i) = 0 \quad (1)$$

$$\frac{\partial}{\partial x_j} (\rho u_i u_j) = -\frac{\partial p}{\partial x_i} + \frac{\partial}{\partial x_j} \left[\mu \left(\frac{\partial u_i}{\partial x_j} + \frac{\partial u_j}{\partial x_i} \right) \right] \quad (2)$$

where x_i ($i = 1, 2$ and 3) are the Cartesian coordinates, u_i is the fluid velocity in the x_i -direction, μ is the molecular viscosity, ρ is the air density, and p is the pressure.

The Navier-Stokes equations are solved using the second-order upwind momentum SIMPLE scheme and the pressure-velocity coupling method. A constant inhalation flow rate can be calculated by [24]:

$$Q_{in} = 2f_b V_t \quad (3)$$

where V_t is the tidal volume, which is defined as the amount of air that flows in and out of the lungs during each respiratory cycle, and f_b is the breathing frequency. Table 2 lists the flow parameters used in this study. The velocity inlet and pressure outlet boundary conditions are considered at the lung model's inlet and outlet, respectively [29–33]. The airway wall was considered to be stationary, and a non-slip boundary condition is used on the wall surface [34–36]. The inhaled air flow rate is considered evenly distributed among all the 2^n bifurcations of generation G-n. As a result, the inlet air flow rate of each inlet of G-n is $Q_e^n = Q_{in}/2^n$, where Q_{in} is the inlet flow rate at G0. Therefore, the inlet velocity of each inlet boundary of G-n is calculated by:

$$u = Q_e^n / A_n \quad (4)$$

where A_n is the cross-sectional area of the inlet.

Table 2. Breathing parameter as a function of age based on the human activity [37].

	Breathing Frequencies f_b (min ⁻¹)	Tidal Volume V_t (mL)	Inhalation Flow Rate Q_{in} (L/min)	Flow Velocity (m/s)	
				Upper Airways (G0–G3)	Lower Airways (G12–G15)
Infant	33.82	47.68	3.22	1.806	0.098
Child	19.34	209.44	8.09	1.766	0.093
Adult	13.98	500	14	1.071	0.080

3.2. Particle Transport Model

The present particle TD model is a one-way coupling model that considers particle movement in airflow but ignores particle effects on the airflow [6]. Initially, the airflow field is simulated to obtain the converged flow solution. Then the particles are injected at the inlet surface into the lung model. The discrete phase model (DPM) model based on the Lagrangian approach is used in this study to model the motion of particles. The equation of motion of each particle is expressed as [6]:

$$\frac{du_i^p}{dt} = F_{Di} + F_{gi} + F_{Bi} + F_{Li} \tag{5}$$

where u_i^p is particle velocity in the x_i -direction, F_{Di} , F_{gi} , F_{Bi} , and F_{Li} are the drag force, gravitational force, Brownian force, and Saffman’s lift force per unit mass. The gravitational force is calculated by

$$F_{gi} = \left(\frac{\rho_p - \rho}{\rho} \right) g_i \tag{6}$$

where g_i is the gravitational acceleration and ρ_p is the density of particles. The drag force is calculated by

$$F_{Di} = \frac{18\mu}{\rho_p d_p^2} C_D \frac{Re_p}{24} (u_i - u_i^p) \tag{7}$$

where the particle Reynolds number $Re_p = \rho d_p |u_i^p - u_i| / \mu$ and the drag coefficient C_D for the spherical particles is calculated by [38] $C_D = a_1 + \frac{a_2}{Re_p} + \frac{a_3}{Re_p^2}$ for $0 < Re_p < 10$. The Brownian force due to Brownian motion of the fluid is defined as

$$F_{Bi} = G_i \sqrt{\frac{\pi S_0}{\Delta t}} \tag{8}$$

where, G_i is zero mean, unit-variance independent Gaussian random number, Δt is the particle time step, and S_0 is the spectral intensity function which is related to the diffusion coefficient by:

$$S_0 = \frac{216\nu k_B T}{\pi^2 \rho_p d_p^2 \left(\frac{\rho_p}{\rho} \right)^2 C_c} \tag{9}$$

where, $T = 300$ K is the absolute fluid temperature, $K_B = 1.380649 \times 10^{-23}$ J/K is the Boltzmann constant, ν is the kinematic viscosity, and the Stokes-Cunningham slip correction coefficient C_c is defined as

$$C_c = 1 + \frac{2\lambda}{d_p} \left(1.257 + 0.4e^{-\left(\frac{1.1d_p}{2\lambda}\right)} \right) \tag{10}$$

where, $\lambda = 65$ nm is the mean free path of the gas molecules. The Saffman’s lift force is calculated by:

$$F_{Li} = \frac{2K\nu^{\frac{1}{2}} \rho d_{ij}}{\rho_p d_p (d_{ik} d_{kl})^{\frac{1}{4}}} (u_j - u_j^p) \tag{11}$$

where, $K = 2.594$ is the constant coefficient of Saffman's lift force and $d_{ij} = (u_{i,j} - u_{j,i})/2$ is the deformation tensor.

In the simulations, 64,400 spherical particles with a uniform diameter and a density of 1100 kg/m^3 were injected randomly at the inlet surface at one time [36,39]. A 'trap' boundary condition is considered in the lung airways wall, and an escape condition is considered at all outputs for particle deposition [28,40]. Due to the trap situation, the coefficient of restitution is zero. Hence no bounce occurs when the particles meet the lung airways surface. As a result, the particles are trapped on the surface and remain there. Finally, the Tecplot software is used to visualize the deposition of particles in the lungs.

3.3. Deposition Efficiency Calculation

The deposition efficiency of the n -th generation, denoted by η , is the percentages of the particles absorbed (trapped) in this generation of airways relative to the particles released at the inlet surface, given by:

$$\eta = \frac{\text{Number of particles are trapped in a lung airway}}{\text{Total number of particles released at the lung inlet}}$$

3.4. Grid Independence Study and Model Validation

3.4.1. Grid Dependency Test

Six meshes are used in the grid independency test, namely 64423 (Mesh-1), 116058 (Mesh-2), 192466 (Mesh-3), 290185 (Mesh-4), 364259 (Mesh-5), and 468164 (Mesh-6). The smallest grid size of the densest mesh is 0.79 mm adjacent to the wall, and the mesh size is proportional to the number of elements. The average velocity magnitude and the total pressure are shown in Figure 3 (the different lines and sections of the lung are defined in Figure 1). It was found that both velocity and pressure change with the increase of the grid number from 64,423 to 468,164. Due to the increased grid number, the velocity distribution trends are almost identical. The velocity difference between mesh-5 and mesh-6, especially, is 0.012%. The average velocity and total pressure converge at a mesh of 364,259 elements (Mesh-5), which is used to perform all the numerical calculations.

3.4.2. Model Validation

To validate the numerical method, Figure 4a,b show the CFD results of particle deposition efficiency as a function of particle diameter for three Reynolds numbers ($Re = 200, 500, \text{ and } 1000$) in the first and second bifurcation areas for G3–G5 model, respectively. The deposition efficiency rate decreases exponentially with the increase of the particle diameter. The variation trend of the deposition efficiency with d_p agrees with those in other numerical studies [7] and experimental data [41], demonstrating that the present model is accurate to calculate the particle TD in the tracheobronchial airways of a lung.

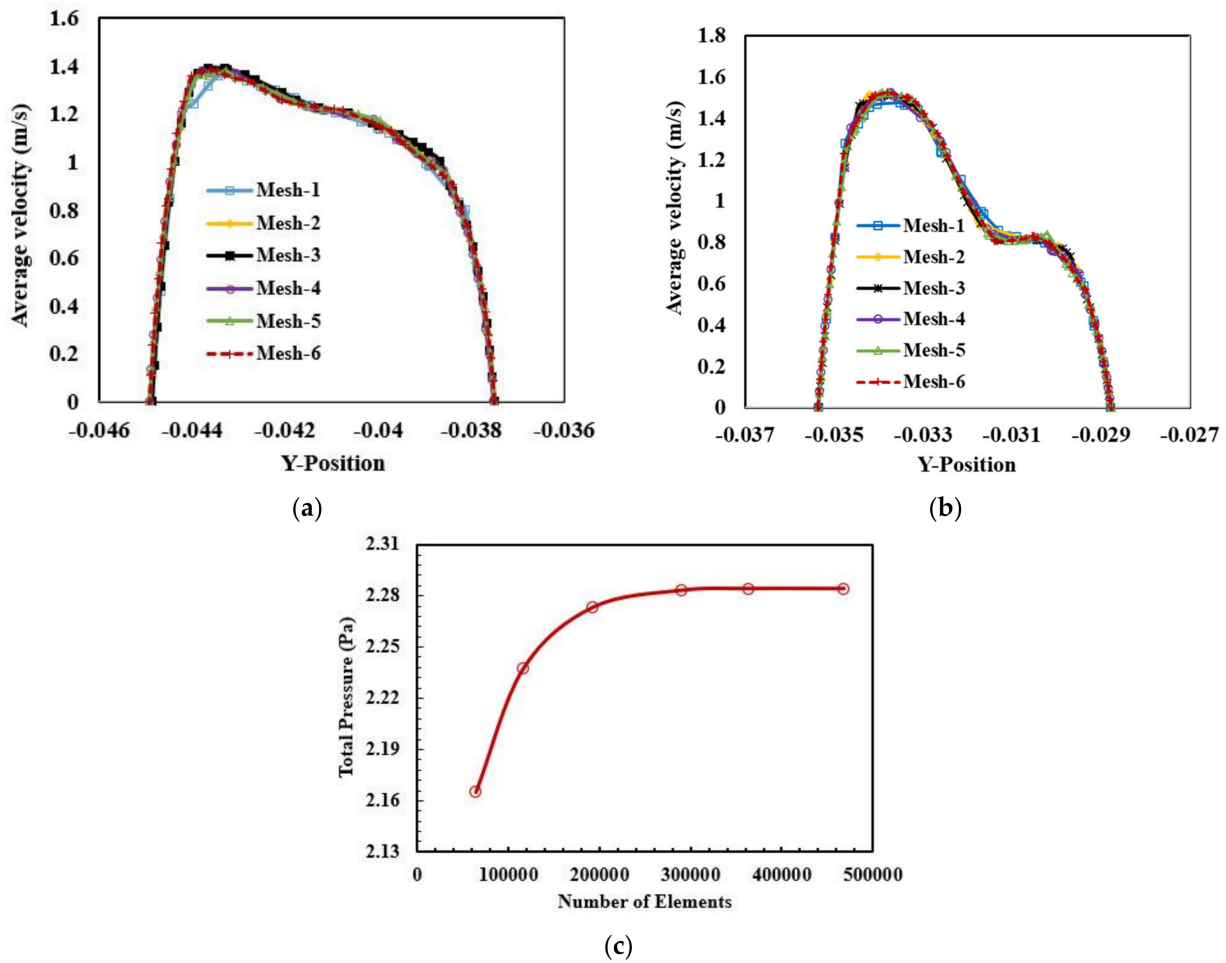


Figure 3. (a) Grid refinement/mesh-independent test for (a) velocity distribution as functions of grid number (average velocity calculated at the selected line-1 in Figure 1), (b) velocity distribution as functions of grid number (average velocity calculated at the selected line-2 in Figure 1), and (c) total pressure as functions of grid number at the flow rate 14 L/min (Total pressure calculated at the selected Section-4 in Figure 1) for G0–G3 model for 30 year age.

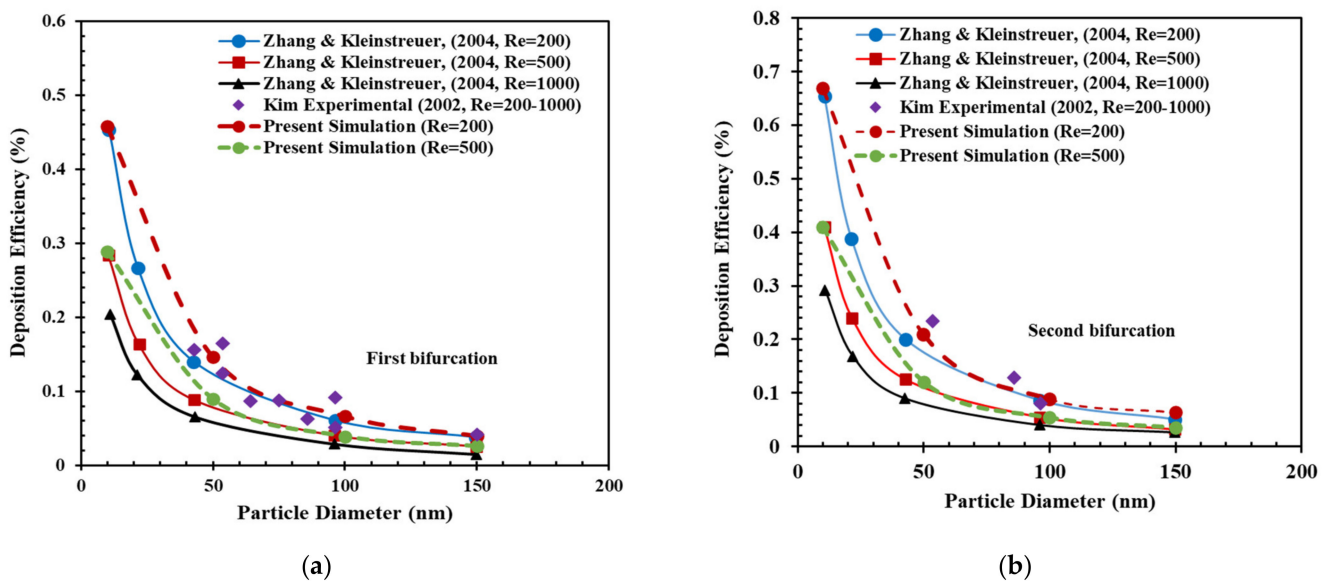


Figure 4. Comparison between present simulation results at the generation G3–G5 model and results from literature [7,41] (a) for the first bifurcation area; and (b) for the second bifurcation area.

4. Results and Discussion

4.1. Airflow Characteristics

In this study, constant velocities at the inlets of the models of G0–G3 and G12–G15 are given based on Table 2. In many studies, the airflow velocity was considered to be constant [42–44].

Figure 5 shows the velocity contours on the symmetric plane and five cross-sections for generation G0–G3 of infants to adults. The five sections (AA', BB', CC', DD', and EE') are indicated on the symmetric plane. The velocity distribution in Section-1 for three ages people is uniform at the central part. After the air enters the deep lung, the velocity distribution in the rest of the section (Sections 2–5) is very non-uniform, as seen in Figure 5. The maximum velocity is observed for 9 months lung model since the lung airways diameter decreases compared to the 30-years age model. There is a qualitatively similar fluctuation in velocity inside the generation G0–G3 compared to the lower generation (G12–G15). According to our observations, lung airway flow rate influences patterns of velocity magnitude.

4.2. Wall Shear Stress

Figure 6 quantitatively shows the average wall shear stress along with the inner wall lung upper airways generation (G0–G3) on five sectional planes indicated in Figure 1. Since flow resistance occurs at complicated lung geometry, the wall shear stress varies considerably with each lung airway generation. With a contact inhaled air flow rate, the wall shear stress decrease with the increase in age.

Figure 7 depicts the average static pressures in the generation G0–G3 lung airways at various locations. For people of all ages, the highest pressure is shown in Section-1 (Figure 7). In addition to the reduction in velocity illustrated in Figure 5, the pressure progressively lowers when airflow enters the deep lung. Due to friction from the inner wall of the airways, the flow energy decreases when the airflow enters the deep lung. The high velocity at the nine-months-old lung shown in Figure 7 requires high pressure at the inlet to drive the flow. As a result, 56.35% pressure rise in the lung airways of 9-month-olds compared to 30-year-olds shown in Figure 7. Hence, inhaling air into the lung for a 9-month-old is more complex than for a 30-year-old. The pressure at Section-5 is significantly lower than at Section-1, owing to a drop in the volume flow rate. As a result of the decrease in velocity, the low-pressure drop-in Section-5 was formed.

4.3. Particle Deposition

Figure 8 shows the effects of age on the particle deposition efficiency in G0–G3 and G12–G15 models. The deposition efficiency of 5-nm particles is much higher than those of the other three-particle diameters. The particle deposition efficiency decreases with the increase of the particle size due to the weakening of the diffusion mechanism [45]. As seen in Table 2, the flow velocity at G12–G15 is reduced significantly compared with G0–G3. Since the diffusion mechanism is strong when the flow velocity is low [46], the deposition efficiency of G12–G15 is 30% higher than that of G0–G3 (Figure 8). Hence, the particles deposition efficiency is found to increase slightly with the increase of age. 2.13% more particles were deposited in the 30-years-old lungs compared to the 9-months-old.

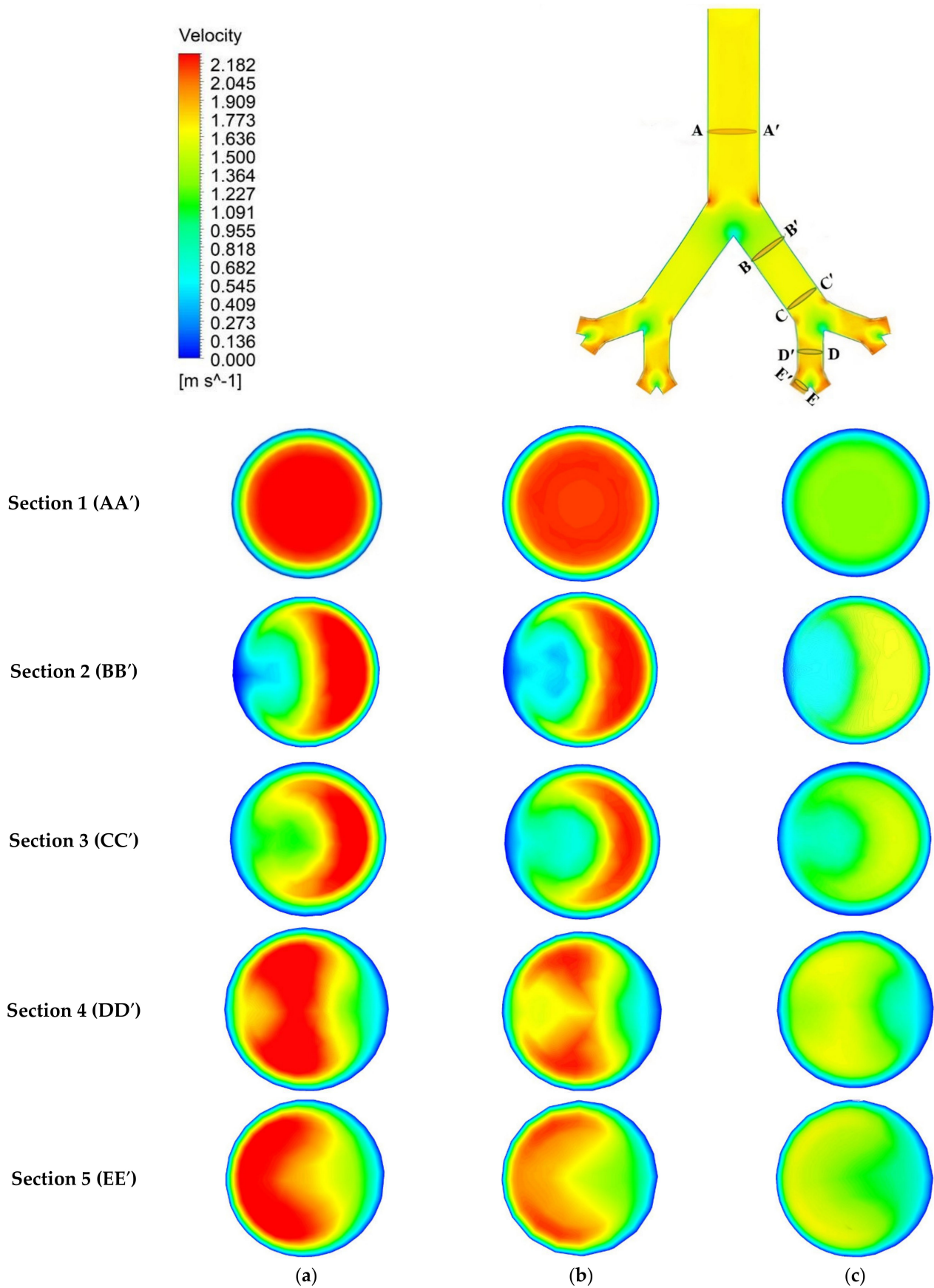


Figure 5. Velocity contours at upper airways generation (G0–G3) defined in the above Figure: (a) 9 months, velocity = 1.806 m/s, (b) 6 years age, velocity = 1.766 m/s, and (c) 30 years age, velocity = 1.071 m/s.

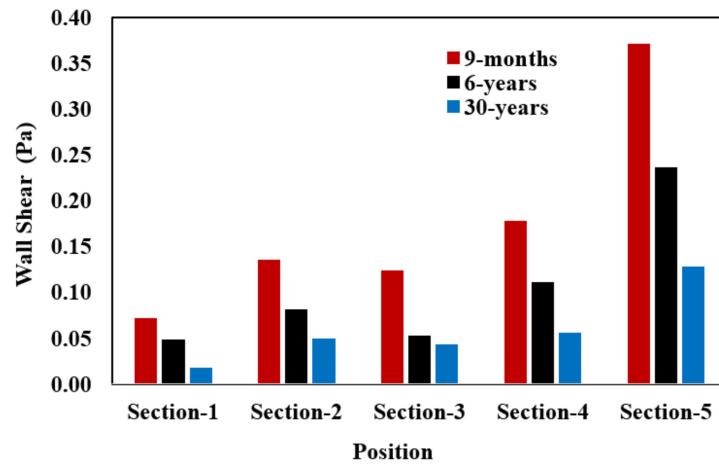


Figure 6. Averaged wall shear stress at a different section of the lung defined in Figure 1 for infant, child and adult ages.

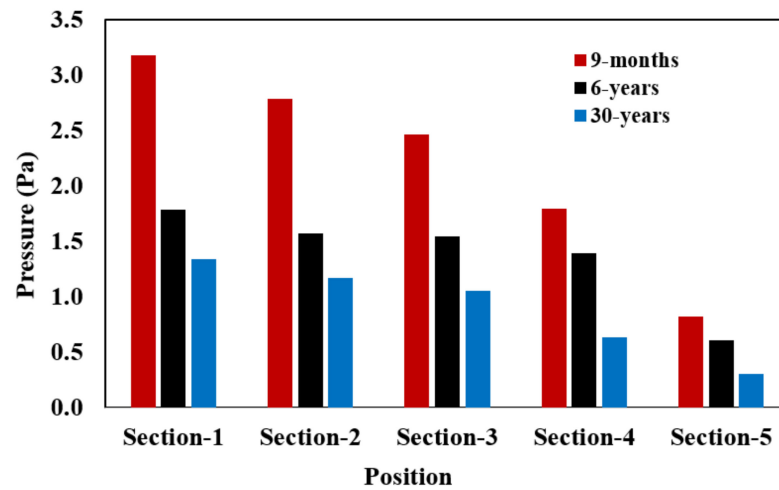


Figure 7. Pressure at a different section of the lung defined in Figure 1 for infant, child, and adult ages.

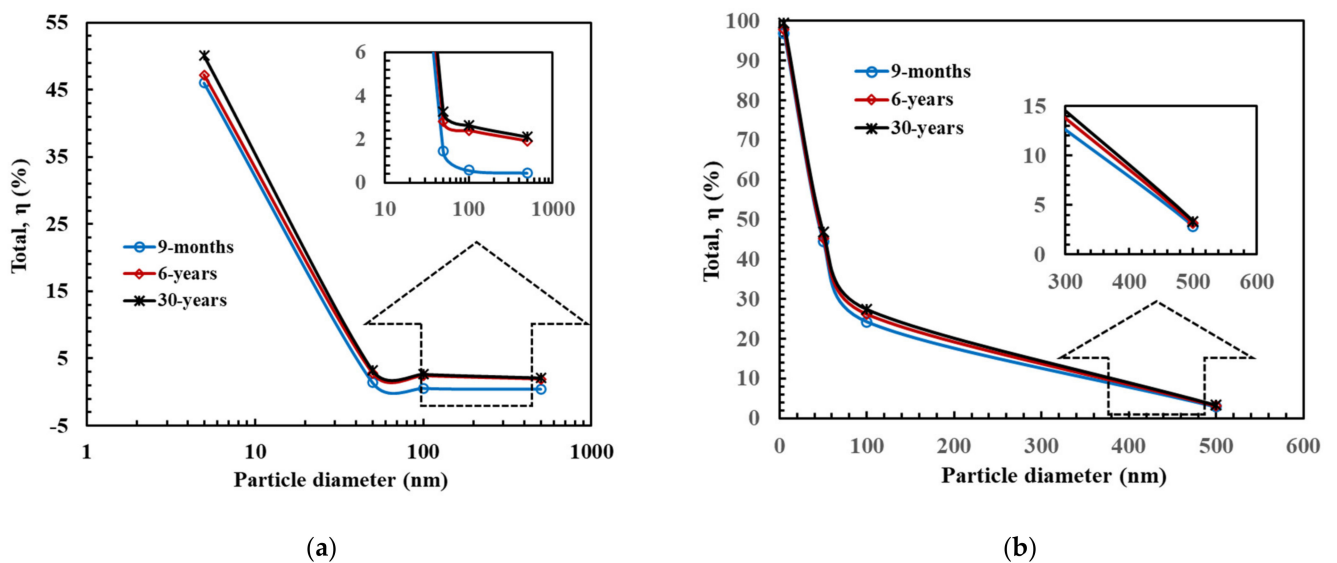


Figure 8. Particle deposition efficiencies of the lung are defined in Figure 1. (a) Upper airways (G0–G3) and (b) lower airways (G12–G15).

Figure 9 shows the visualization of the particle distribution of different sized particles at generation G12–G15 of 30-year age. The calculated total particle deposition efficiencies of G12–G15 are 99.42%, 46.80%, 27.45%, and 3.33% for 5 nm, 50 nm, 100 nm, and 500 nm particles, respectively. It can be found that 5 nm particles are more evenly distributed in each lung airways generation compared to the larger particles (500 nm). Hence, 500 nm size particle is observed to have less deposition than smaller diameters since the diffusion mechanism weakens with the increase of particle diameter. The Brownian diffusion mechanism results in more particles being deposited due to the low airflow velocity [7,14].

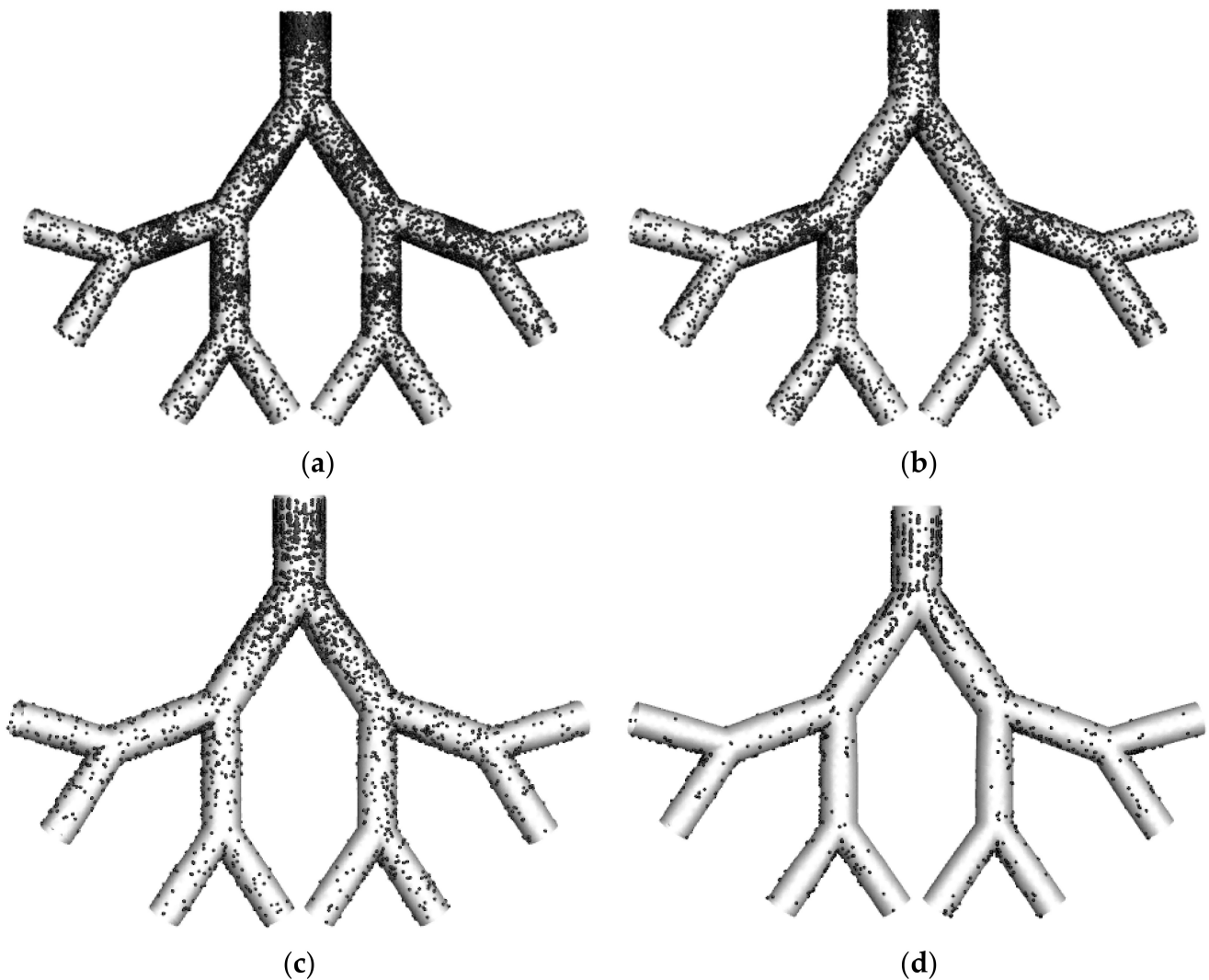


Figure 9. Visualization of particle deposition for the 30 years age for generation G12–G15 of the lung defined in Figure 1. (a) $d_p = 5$ nm, (b) $d_p = 50$ nm, (c) $d_p = 100$ nm, and (d) $d_p = 500$ nm at a flow rate of 14 L/min.

How the ages and particle size affect deposition rates at individual generations in the upper lung airways (G0–G3) can be examined by the bar charts shown in Figure 10. The locations of different generations are defined in Figure 1. Most of the particles are deposited at generation G0 for all the studied ages and particle diameters. Around 34.88%, 35.67%, and 37.72% of 5 nm particles are deposited at generation G0 for 9-month, 6-years and 30-years of age, respectively (Figure 10a). For the three ages, the lowest deposition efficiency occurs at the largest particle size of 500 nm and it decreases with the increase of generation number. Figure 4 demonstrates that the deposition efficiency in generations G3–G5 increases with the reduction of either the Reynolds number or flow velocity. The de-

crease of the flow velocity decreases with age results in an increase in deposition efficiency in G0–G3 in Figure 10.

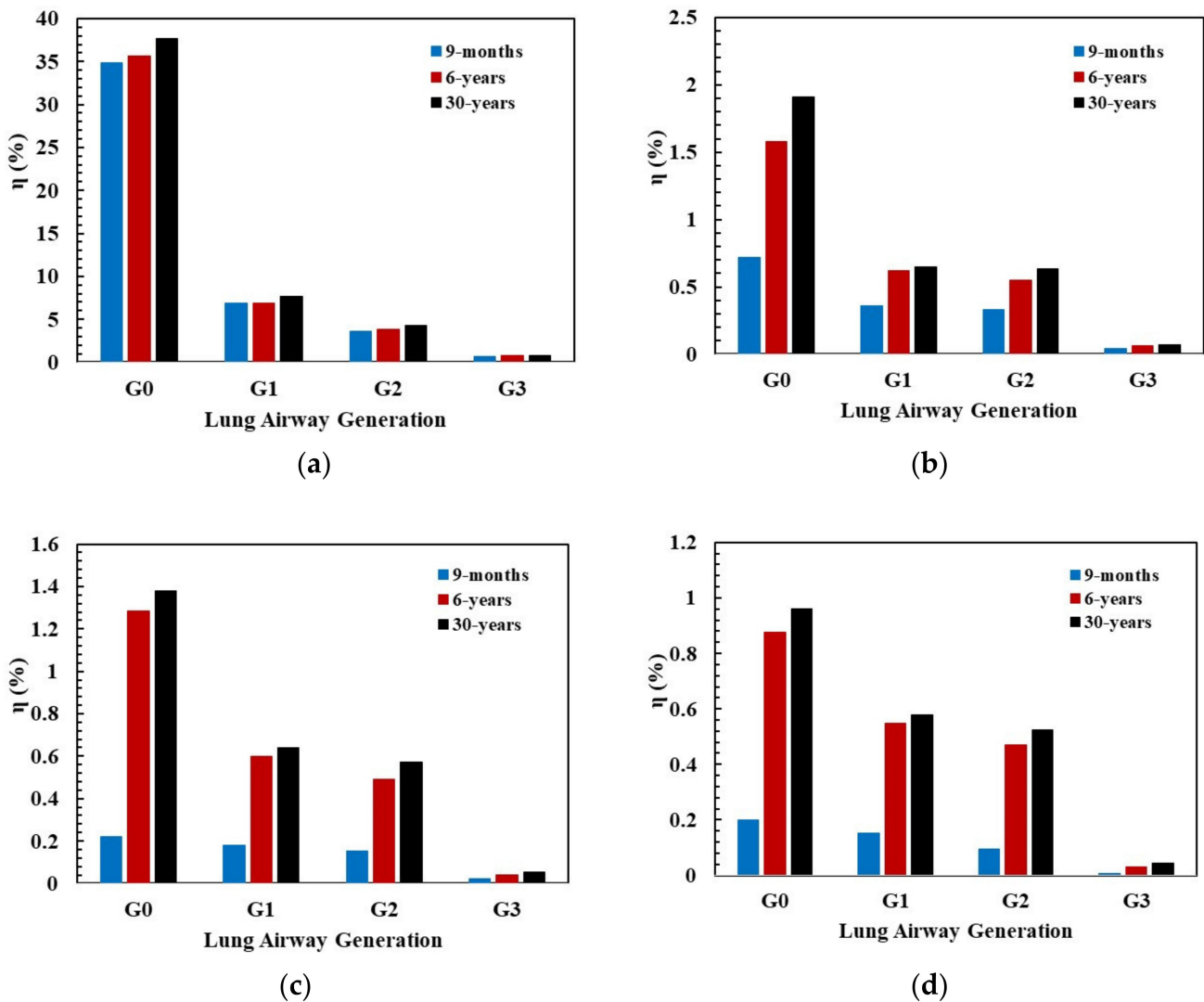


Figure 10. Different size particle deposition efficiencies at upper airways generation (G0–G3) of the lung are defined in Figure 1. (a) $d_p = 5$ nm, (b) $d_p = 50$ nm, (c) $d_p = 100$ nm, and (d) $d_p = 500$ nm.

Figure 11 shows the deposition efficiency at individual generations in the lower lung airways (G12–G15) for the three ages. The effect of age on the deposition efficiency of G12–G15 is the same as that for G0–G3. At nine-months of age, the deposition efficiencies of lower generations (G15) are smaller compared to the adult age. The deposition efficiency in G12–G15 for all the diameters was considerably reduced compared to that in G0–G3. At 9-month age, 15.61%, 14.05%, 12.71%, and 1.57% of 50 nm particles are deposited at the generation G12, G13, G14, and G15, respectively (Figure 11b). It is also observed that 8.02% at G12, 7.54% at G13, 6.37% at G14, and 1.16% at G15, more particles were deposited of 100 nm compared to 500 nm for six-year-olds (Figure 11c,d). The particles deposition efficiency decreases with increases the particles size (Figure 11a).

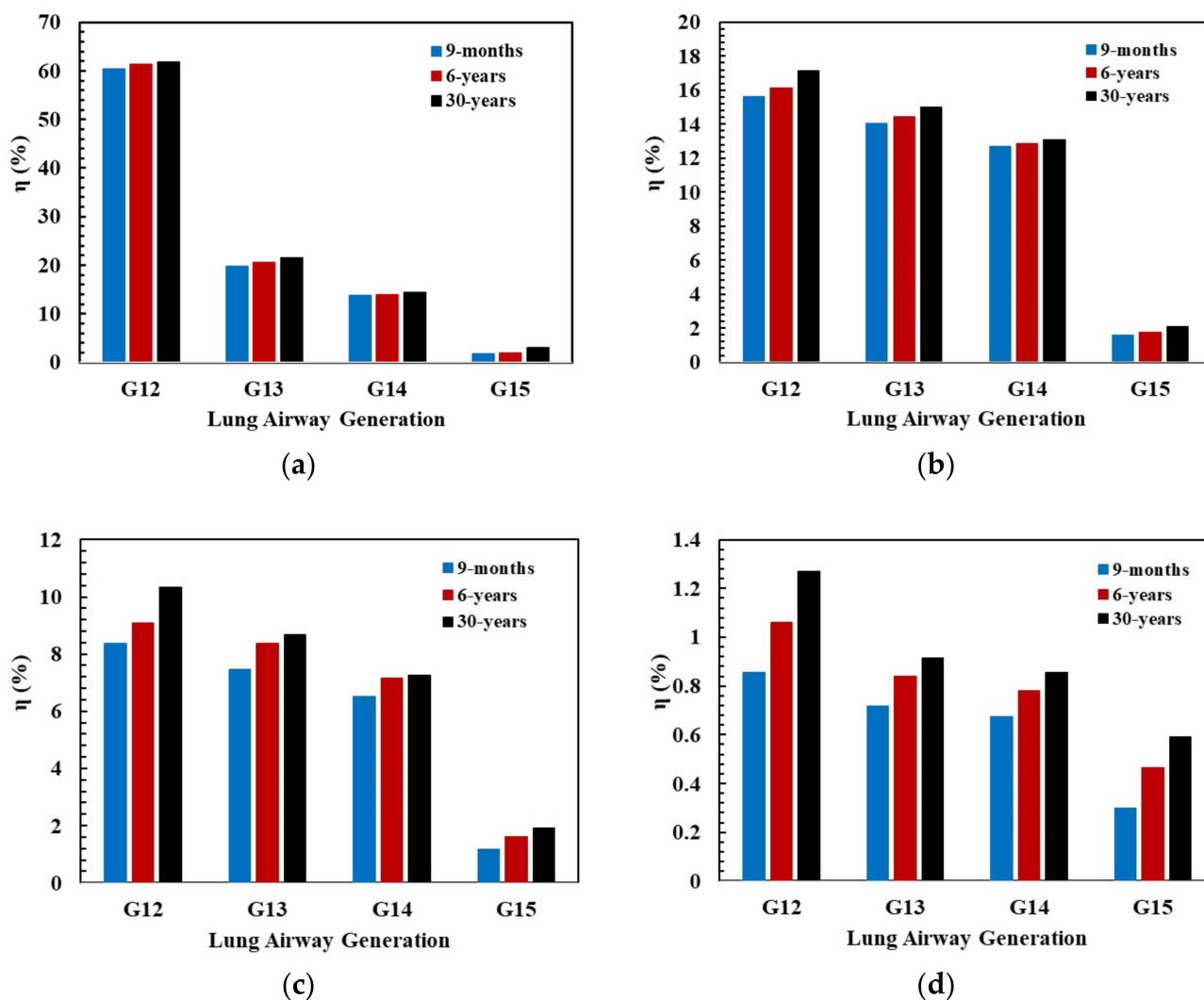


Figure 11. Different size particle deposition efficiencies at lower airways generation (G12–G15) of the lung are defined in Figure 1. (a) $d_p = 5$ nm, (b) $d_p = 50$ nm, (c) $d_p = 100$ nm, and (d) $d_p = 500$ nm.

Numerical calculations were conducted based on age-specific lung models in the upper and lower airways. The flow characteristics and pressures differ due to age-related differences in lung geometries that have varied diameters. Due to lung aging and flow rate, the diameter reduction influenced the velocity magnitude for infant to adult ages. Hence, the present study has several contributions: (1) we have considered the three age groups (infant, child, and adult) to identify the effects of age on particle TD; (2) we consider the nanoparticle TD through diffusion mechanism both in upper (G0–G3) and lower (G12–G15) airways; (3) we consider the different airflow velocity in different airway generations.

4.4. Limitations of the Study

There are some limitations in this study that should be addressed in future studies. Firstly, only an inhalation flow condition was considered in the simulation of particle TD. Secondly, deformation of the lung wall was not considered in this study. Thirdly, we have used symmetric and planner lung airways models due to the lack of high-resolution CT images for age-specific realistic lung geometry. However, despite the constraints of lung geometry used in this study, our current investigation of airflow characteristics and particle deposition patterns can accurately predict [42,47]. Thus, the results of this work could improve a basic understanding of airflow properties and nanoparticle TD in the human lung airways related to lung aging.

5. Conclusions

We investigated nanoparticle TD in the upper (G0–G3) and lower (G12–G15) airways of the infant to adult ages. The variation of the airway geometry and the flow velocity with age has been considered. The deposition efficiency of particles is found to be significantly affected by lung airways reduction. The effects of age and particle diameter on the airflow and particle TD are summarized as follows.

- The average wall shear stress is decreased with an increase of age. The pressure of generation G0 to G3 of a 9-month-old lung is 56.35% higher than the 30-year-old lung due to the inhalation flow rate.
- 30% more particles are deposited in the lower airways (G12–G15) than in the upper airways (G0–G3).
- 60.32%, 61.31%, and 61.75% 5-nm particles are deposited in the generation G12 for 9-month, 6-year, and 30-year ages, respectively, which indicates that the number of particle deposition increases with increased age.
- A high percentage of the 5-nm particles (over 95%) entering G12 can be deposited in the deep lung airways (G12–G15). As the particle size is increased to 500 nm, only 3% of the particles are deposited in the G12–G15 lung airways. The above finding indicates that particles must have a small diameter to increase the deposition in the deep lung airways.
- The numerical study showed that deposition efficiency is significantly affected by lung airways reduction. Most of the particles are deposited in the 30-year-old lung than 9-month-old lung in the lower generations compared to the upper generation. Therefore, our results further investigate that correctly choosing particles size as targeted drug-aerosol delivery size based on age.

Author Contributions: Conceptualization, M.M.R.; Formal analysis, M.M.R.; Investigation, M.M.R. and M.Z.; Methodology, M.M.R. and M.Z.; Software, M.M.R. and M.S.I.; Supervision, M.Z., M.S.I., K.D. and S.C.S.; Validation, M.M.R.; Visualization, M.Z.; Writing—original draft, M.M.R.; Writing—review & editing, M.Z., M.S.I., K.D. and S.C.S. All authors have read and agreed to the published version of the manuscript.

Funding: This research received no external funding.

Institutional Review Board Statement: Not applicable.

Informed Consent Statement: Informed consent was obtained from all subjects involved in the study.

Acknowledgments: M.M.R. would like to thank the support of International Post-graduate Research Scholarship (IPRS) through Australian Government Research Training Program. The authors also acknowledge that the WSU High-Performance VM machine provided the computational facilities.

Conflicts of Interest: The authors state no conflict of interest.

References

1. Sorino, C.; Negri, S.; Spanevello, A.; Visca, D.; Scichilone, N. Inhalation therapy devices for the treatment of obstructive lung diseases: The history of inhalers towards the ideal inhaler. *Eur. J. Intern. Med.* **2020**, *75*, 15–18. [[CrossRef](#)]
2. Pulivendala, G.; Bale, S.; Godugu, C. Inhalation of sustained release microparticles for the targeted treatment of respiratory diseases. *Drug Deliv. Transl. Res.* **2020**, *10*, 339–353. [[CrossRef](#)]
3. Matera, M.G.; Calzetta, L.; Ora, J.; Rogliani, P.; Cazzola, M. Pharmacokinetic/pharmacodynamic approaches to drug delivery design for inhalation drugs. *Expert Opin. Drug Deliv.* **2021**, *18*, 891–906. [[CrossRef](#)] [[PubMed](#)]
4. Saha, S.; Islam, M.S.; Luo, Z. Ultrafine particle transport and deposition in the upper airways of a CT-based realistic lung. In Proceedings of the 21st Australasian Fluid Mechanics Conference (AFMC 2018), Adelaide, Australia, 10–13 December 2018.
5. Wang, J.; Fan, Y. Lung injury induced by TiO₂ nanoparticles depends on their structural features: Size, shape, crystal phases, and surface coating. *Int. J. Mol. Sci.* **2014**, *15*, 22258–22278. [[CrossRef](#)]
6. Inthavong, K.; Zhang, K.; Tu, J. Numerical modelling of nanoparticle deposition in the nasal cavity and the tracheobronchial airway. *Comput. Methods Biomech. Biomed. Eng.* **2011**, *14*, 633–643. [[CrossRef](#)] [[PubMed](#)]
7. Zhang, Z.; Kleinstreuer, C. Airflow structures and nano-particle deposition in a human upper airway model. *J. Comput. Phys.* **2004**, *198*, 178–210. [[CrossRef](#)]

8. Islam, M.S.; Larpruenrudee, P.; Saha, S.C.; Pourmehran, O.; Paul, A.R.; Gemci, T.; Collins, R.; Paul, G.; Gu, Y. How severe acute respiratory syndrome coronavirus-2 aerosol propagates through the age-specific upper airways. *Phys. Fluids* **2021**, *33*, 081911. [[CrossRef](#)]
9. Cheng, K.-H.; Cheng, Y.-S.; Yeh, H.-C.; Swift, D. Measurements of airway dimensions and calculation of mass transfer characteristics of the human oral passage. *J. Biomech. Eng.* **1997**, *119*, 476–482. [[CrossRef](#)]
10. Balásházy, I.; Hofmann, W. Deposition of aerosols in asymmetric airway bifurcations. *J. Aerosol Sci.* **1995**, *26*, 273–292. [[CrossRef](#)]
11. Weibel, E.R.; Cournand, A.F.; Richards, D.W. *Morphometry of the Human Lung*; Springer: Berlin/Heidelberg, Germany, 1963.
12. Moskal, A.; Gradoń, L. Temporary and spatial deposition of aerosol particles in the upper human airways during breathing cycle. *J. Aerosol Sci.* **2002**, *33*, 1525–1539. [[CrossRef](#)]
13. Hofmann, W.; Golser, R.; Balashazy, I. Inspiratory deposition efficiency of ultrafine particles in a human airway bifurcation model. *Aerosol Sci. Technol.* **2003**, *37*, 988–994. [[CrossRef](#)]
14. Pourmehran, O.; Gorji, T.B.; Gorji-Bandpy, M. Magnetic drug targeting through a realistic model of human tracheobronchial airways using computational fluid and particle dynamics. *Biomech. Modeling Mechanobiol.* **2016**, *15*, 1355–1374. [[CrossRef](#)]
15. Islam, M.S.; Saha, S.C.; Sauret, E.; Gemci, T.; Yang, I.A.; Gu, Y. Ultrafine particle transport and deposition in a large scale 17-generation lung model. *J. Biomech.* **2017**, *64*, 16–25. [[CrossRef](#)]
16. Asgari, M.; Lucci, F.; Kuczaj, A.K. Multispecies aerosol evolution and deposition in a human respiratory tract cast model. *J. Aerosol Sci.* **2021**, *153*, 105720. [[CrossRef](#)]
17. Ménache, M.; Hofmann, W.; Ashgarian, B.; Miller, F. Airway geometry models of children’s lungs for use in dosimetry modeling. *Inhal. Toxicol.* **2008**, *20*, 101–126. [[CrossRef](#)] [[PubMed](#)]
18. Veneroni, C.; Mercadante, D.; Lavizzari, A.; Colnaghi, M.; Mosca, F.; Dellacà, R.L. Changes in respiratory mechanics at birth in preterm infants: A pilot study. *Pediatric Pulmonol.* **2020**, *55*, 1640–1645. [[CrossRef](#)]
19. Anderko, L.; Chalupka, S.; Du, M.; Hauptman, M. Climate changes reproductive and children’s health: A review of risks, exposures, and impacts. *Pediatr. Res.* **2020**, *87*, 414–419. [[CrossRef](#)]
20. Kim, J.B.; Prunicki, M.; Haddad, F.; Dant, C.; Sampath, V.; Patel, R.; Smith, E.; Akdis, C.; Balmes, J.; Snyder, M.P. Cumulative lifetime burden of cardiovascular disease from early exposure to air pollution. *J. Am. Heart Assoc.* **2020**, *9*, e014944. [[CrossRef](#)]
21. Vriesman, M.H.; Koppen, I.J.; Camilleri, M.; Di Lorenzo, C.; Benninga, M.A. Management of functional constipation in children and adults. *Nat. Rev. Gastroenterol. Hepatol.* **2020**, *17*, 21–39. [[CrossRef](#)]
22. Schechter, M.S. Airway clearance applications in infants and children. *Respir. Care* **2007**, *52*, 1382–1391. [[PubMed](#)]
23. Xu, G.; Yu, C. Effects of age on deposition of inhaled aerosols in the human lung. *Aerosol Sci. Technol.* **1986**, *5*, 349–357. [[CrossRef](#)]
24. Deng, Q.; Ou, C.; Chen, J.; Xiang, Y. Particle deposition in tracheobronchial airways of an infant, child and adult. *Sci. Total Environ.* **2018**, *612*, 339–346. [[CrossRef](#)]
25. Rahman, M.M.; Zhao, M.; Islam, M.S.; Dong, K.; Saha, S.C. Aging effects on airflow distribution and micron-particle transport and deposition in a human lung using CFD-DPM approach. *Adv. Powder Technol.* **2021**, *32*, 3506–3516. [[CrossRef](#)]
26. Kwok, P.C.L.; Chan, H.-K. Delivery of inhalation drugs to children for asthma and other respiratory diseases. *Adv. Drug Deliv. Rev.* **2014**, *73*, 83–88. [[CrossRef](#)] [[PubMed](#)]
27. Knoppert, D.; Reed, M.; Benavides, S.; Totton, J.; Hoff, D.; Moffett, B.; Norris, K.; Vaillancout, R.; Aucoin, R.; Worthington, M. Paediatric age categories to be used in differentiating between listing on a model essential medicines list for children. *World Health Organ. Position Pap.* **2007**, *1*, 1–5.
28. Zhang, W.; Xiang, Y.; Lu, C.; Ou, C.; Deng, Q. Numerical modeling of particle deposition in the conducting airways of asthmatic children. *Med. Eng. Phys.* **2020**, *76*, 40–46. [[CrossRef](#)]
29. Islam, M.S.; Saha, S.C.; Sauret, E.; Ong, H.; Young, P.; Gu, Y. Euler–Lagrange approach to investigate respiratory anatomical shape effects on aerosol particle transport and deposition. *Toxicol. Res. Appl.* **2019**, *3*, 2397847319894675. [[CrossRef](#)]
30. Singh, P.; Raghav, V.; Padhmashali, V.; Paul, G.; Islam, M.S.; Saha, S.C. Airflow and particle transport prediction through stenosis airways. *Int. J. Environ. Res. Public Health* **2020**, *17*, 1119. [[CrossRef](#)]
31. Ghosh, A.; Islam, M.S.; Saha, S.C. Targeted drug delivery of magnetic nano-particle in the specific lung region. *Computation* **2020**, *8*, 10. [[CrossRef](#)]
32. Gu, Q.; Qi, S.; Yue, Y.; Shen, J.; Zhang, B.; Sun, W.; Qian, W.; Islam, M.S.; Saha, S.C.; Wu, J. Structural and functional alterations of the tracheobronchial tree after left upper pulmonary lobectomy for lung cancer. *Biomed. Eng. Online* **2019**, *18*, 1–18. [[CrossRef](#)]
33. Rahman, M.M.; Zhao, M.; Islam, M.S.; Dong, K.; Saha, S.C. Airflow dynamic and particle deposition in age-specific human lungs. In Proceedings of the 22nd Australasian Fluid Mechanics Conference (AFMC 2020), Brisbane, Australia, 7–10 December 2020.
34. Islam, M.S.; Larpruenrudee, P.; Hossain, S.I.; Rahimi-Gorji, M.; Gu, Y.; Saha, S.C.; Paul, G. Polydisperse Aerosol Transport and Deposition in Upper Airways of Age-Specific Lung. *Int. J. Environ. Res. Public Health* **2021**, *18*, 6239. [[CrossRef](#)]
35. Hendryx, M.; Islam, M.S.; Dong, G.-H.; Paul, G. Air pollution emissions 2008–2018 from Australian coal mining: Implications for public and occupational health. *Int. J. Environ. Res. Public Health* **2020**, *17*, 1570. [[CrossRef](#)]
36. Islam, M.S.; Gu, Y.; Farkas, A.; Paul, G.; Saha, S.C. Helium–oxygen mixture model for particle transport in CT-based upper airways. *Int. J. Environ. Res. Public Health* **2020**, *17*, 3574. [[CrossRef](#)] [[PubMed](#)]
37. Hofmann, W. Mathematical model for the postnatal growth of the human lung. *Respir. Physiol.* **1982**, *49*, 115–129. [[CrossRef](#)]
38. Morsi, S.; Alexander, A. An investigation of particle trajectories in two-phase flow systems. *J. Fluid Mech.* **1972**, *55*, 193–208. [[CrossRef](#)]

39. Rahman, M.M.; Zhao, M.; Islam, M.S.; Dong, K.; Saha, S.C. Numerical study of nanoscale and microscale particle transport in realistic lung models with and without stenosis. *Int. J. Multiph. Flow* **2021**, *145*, 103842. [[CrossRef](#)]
40. Rahman, M.M.; Zhao, M.; Islam, M.S.; Dong, K.; Saha, S.C. Airflow dynamics and aerosol particle transport in a human lung. In Proceedings of the 1st International Conference on Mechanical and Manufacturing Engineering Research and Practice (iCMMERP-2019), Sydney, Australia, 24–28 November 2019; pp. 5–9.
41. Kim, C. *Ultrafine Particle Deposition in a Double Bifurcation Tube with Human G3–G5 Airway Geometry*; Internal Report; US EPA: Washington, DC, USA, 2002.
42. Kleinstreuer, C.; Zhang, Z.; Li, Z. Modeling airflow and particle transport/deposition in pulmonary airways. *Respir. Physiol. Neurobiol.* **2008**, *163*, 128–138. [[CrossRef](#)]
43. Chen, X.; Feng, Y.; Zhong, W.; Sun, B.; Tao, F. Numerical investigation of particle deposition in a triple bifurcation airway due to gravitational sedimentation and inertial impaction. *Powder Technol.* **2018**, *323*, 284–293. [[CrossRef](#)]
44. Islam, M.S.; Larpruenrudee, P.; Paul, A.R.; Paul, G.; Gemci, T.; Gu, Y.; Saha, S.C. SARS CoV-2 aerosol: How far it can travel to the lower airways? *Phys. Fluids* **2021**, *33*, 061903. [[CrossRef](#)]
45. Dong, J.; Shang, Y.; Tian, L.; Inthavong, K.; Qiu, D.; Tu, J. Ultrafine particle deposition in a realistic human airway at multiple inhalation scenarios. *Int. J. Numer. Methods Biomed. Eng.* **2019**, *35*, e3215. [[CrossRef](#)]
46. Dang Khoa, N.; Phuong, N.L.; Ito, K. Numerical modeling of nanoparticle deposition in realistic monkey airway and human airway models: A comparative study. *Inhal. Toxicol.* **2020**, *32*, 311–325. [[CrossRef](#)]
47. Ou, C.; Jian, H.; Deng, Q. Particle Deposition in Human Lung Airways: Effects of Airflow, Particle Size, and Mechanisms. *Aerosol Air Qual. Res.* **2020**, *20*, 2846–2858. [[CrossRef](#)]